Experimental and numerical investigation on thermal performance enhancement of phase change material embedding porous metal structure with cubic cell

Xusheng Hu, Xiao-Lu Gong

▶ **To cite this version:**

Xusheng Hu, Xiao-Lu Gong. Experimental and numerical investigation on thermal performance enhancement of phase change material embedding porous metal structure with cubic cell. Applied Thermal Engineering, 2020, pp.115337. 10.1016/j.applthermaleng.2020.115337 . hal-02550742v2

HAL Id: hal-02550742
https://utt.hal.science/hal-02550742v2

Submitted on 22 Aug 2022

HAL is a multi-disciplinary open access archive for the deposit and dissemination of scientific research documents, whether they are published or not. The documents may come from teaching and research institutions in France or abroad, or from public or private research centers.

L'archive ouverte pluridisciplinaire **HAL**, est destinée au dépôt et à la diffusion de documents scientifiques de niveau recherche, publiés ou non, émanant des établissements d'enseignement et de recherche français ou étrangers, des laboratoires publics ou privés.

Distributed under a Creative Commons Attribution - NonCommercial 4.0 International License

Version of Record: https://www.sciencedirect.com/science/article/pii/S1359431119384388
Manuscript_868048325f8f82895ed9ff67db3fc875

Experimental and numerical investigation on thermal performance enhancement of phase change material embedding porous metal structure with cubic cell

Xusheng Hu, Xiaolu Gong*
Charles Delaunay Institute, LASMIS, University of Technology of Troyes, 12 Rue Marie Curie, 10004 Troyes, France
(*) Correspondent author, gong@utt.fr

Abstract

Phase change material (PCM) is a promising candidate for application to thermal energy storage. However, low thermal conductivity hinders its wide application. In this paper, a porous metal structure (PMS) with cubic cell is used to enhance the thermal performance of PCM, in which additive manufacturing (AM) as advanced manufacturing technology enables the fast and precise fabrication of PMS with a controlled structure and material. A visualized experiment setup is built to investigate the thermal performance of PCM with and without PMS, including solid-liquid interface, temperature variation, and total melting time. To examine the heat transfer characteristics and clarify the role of PMS in the melting process, a three-dimensional numerical model is developed based on the pore-scale numerical simulation method. The experimental results illustrate that embedding PMS can significantly improve the thermal performance of PCM, e.g., the total melting time can be shortened by 38% compared with that for PCM without PMS. The numerical results are in good agreement with experimental results, which indicates that heat transfer characteristics can be predicted using pore-scale numerical simulation. The numerical results show that the temperature field of PCM with PMS is more uniform and heat transfer mechanics is different for PCM with and without PMS. In addition, PMS made of highly thermally conductive materials significantly enhances the thermal performance of PCM. Due to structure and material controllability of porous material fabricated by AM, this study highlights the capacity and potential of PMS as a heat transfer enhancer.

Keywords: Phase change material; Porous metal structure; Additive manufacturing; Pore-scale numerical simulation; Thermal performance

© 2020 published by Elsevier. This manuscript is made available under the CC BY NC user license
https://creativecommons.org/licenses/by-nc/4.0/

Nomenclature

A_{mush}	mush constant	T	temperature (K)
a	ligament thickness (m)	t	time (s)
C	specific heat capacity (J/kg K)	u	velocity (m/s)
c	smaller constant		
f_l	liquid fraction	Greek symbols	
Gr	Grashof number	ε	porosity
g	gravitational acceleration (m/s^2)	β	thermal expansion coefficient (1/K)
h	heat transfer coefficient (W/m^2 K)	μ	dynamic viscosity (kg/m s)
k	thermal conductivity (W/m K)	ρ	density (kg/m^3)
L	latent heat (J/kg K)		
l	ligament length (m)	Subscripts	
P	pressure (Pa)	p	paraffin
Pr	Prandtl number	s	metal structure
$\dot{q}$	heat generation rate (W/m^3)	w	wall
S	source term	m	melting

1. Introduction

Phase change material (PCM) has been widely applied in thermal energy storage (TES) and thermal management system (TMS) owing to its considerable phase change latent heat, appropriate phase transition temperature, and chemical stability [1, 2]. However, most PCMs suffer from low thermal conductivities, which results in low heat transfer rate and distinct heat accumulation near the heated wall (i.e., temperature non-uniformity) [3, 4]. As a result, researchers make efforts to develop the various enhancement techniques which can be used to improve the thermal performance of PCMs. The extensively employed enhancement methods include using a high thermal conductivity additive [5-8], inserting metal fin and pin [9-11], encapsulation of PCMs [12-14], and embedding porous metal material [15-18].

Among the above methods, embedding porous metal material has proven to be an efficient approach to heighten the thermal behavior of PCM due to its light weight, larger specific surface, and high thermal conductivity. The porous metal material is mainly classified into two broad classes, one with stochastic topology (i.e., metal foam) and the other with a periodic cell structure [19, 20]. As a commercial porous material, open-cell metal foam is infiltrated with PCM to fabricate metal foam/paraffin composite PCM. Several studies on the thermal behavior and application of PCM saturated in metal foam have been conducted [21-23]. For instance, Yang et al. [24] implemented a numerical and experimental study on the solidification of PCM impregnated in open-cell metal foam. They concluded that temperature difference between PCM and metal skeleton was negligible, and local thermal equilibrium model can be employed. Based on pore-scale and volume-averaged numerical simulation methods, the phase change characteristics of PCM impregnated in finned metal foam were numerically explored by Feng et al. [25]. An experimental and numerical investigation on melting heat transfer of metal foam/paraffin composite PCM was conducted by Zhang et al. [26]. Rehman et al. [27] designed a copper foam/paraffin based heat sink used for an electronic cooling system, and carried out an

experimental study on thermal behavior of the heat sink. Li et al. [28] experimentally examined thermophysical properties of copper foam/hydrate salts PCM composite applied for thermal energy storage. They found that volume storage energy density of PCM composite is 2.2-2.5 times of that of conventional water tank.

The open literature indicates that embedding porous metal structure (PMS) with a periodic cell structure is capable of heightening thermal behavior of PCM. The structured porous media was used as the thermal conductivity enhancer, and heat transfer enhancement of PCM embedding porous structure with different configurations was numerically investigated by Gopalan et al. [29]. In our previous study, we performed a numerical study on the thermal behavior of PCM infiltrated in porous material with cubic periodic structure [30]. The results indicated that impregnation of PMS into PCM can strengthen the thermal performance of PCM. For instance, the effective thermal conductivity of composite PCM clearly increased, and melting time of composite PCM can be shortened to 24.1% of that of pure paraffin. Research on the thermal performance of PCM embedding PMS remains rare compared to embedding metal foam. In addition, the porous metal structure is difficult to manufacture by traditional fabrication techniques owing to its special and complex configuration, which also explains the lack of related experimental investigation.

Additive manufacturing (i.e., 3D printing) can fabricate intricate three-dimensional (3D) structure by successive printing thin layers of materials according to 3D model data, which provides a means to quickly and precisely manufacture PMS based on a customization or an optimization model [31, 32]. For example, Merabtine et al. [33] carried out an experimental and numerical study on thermal behavior for PCM saturated in PMS, in which PMS was developed by topological optimization and fabricated via 3D printing. They found that the pore size and porosities of porous structure had a significant influence on heat transfer within composite PCM. Porous metal structure is a particularly promising candidate as an enhancer of composite PCM due to its controllable geometrical structure through the introduction of 3D printing. Thus, the study of thermal performance of PCM infiltrated in PMS is of great significance.

Porous metal structure can be manufactured by 3D printing using a wide variety of materials, such as aluminum alloy, copper alloy, stainless steel, etc. With the development of additive manufacturing material, 3D printing has exhibited significant potential for the fabrication of PMS using various printing materials. Therefore, four representative metal materials used in 3D printing are chosen here (i.e., aluminum alloy, copper alloy, titanium alloy, and stainless steel) to investigate the influence of materials of PMS on thermal performance of composite PCM. In this paper, a PMS with a cubic cell structure was fabricated by the selective laser melting (SLM) as one of 3D printing techniques. The heat transfer characteristics of PCM with and without PMS were experimentally and numerically investigated, including the evolution of solid-liquid interface, liquid fraction, temperature field, velocity field, enhancement ratio, etc. Furthermore, the effect of materials of PMS on the thermal behavior of composite PCMs was explored based on pore-scale numerical simulation, which provides a reference for

the choice of materials of PMS as heat transfer enhancer.

2. Experiment details

2.1. Test samples

As shown in Fig. 1, a porous aluminum structure with dimensions of $40\ \text{mm}\times40\ \text{mm}\times40\ \text{mm}$ was used as enhancement material in this study. The sample was composed of aluminum alloy with a high thermal conductivity using SLM, where the manufacturing accuracy of 3D printing was 50-100 μm. It is seen that porous aluminum material possesses a periodic cubic cell structure, and the metal ligament was connected at angles of 90°. The length and thickness of metal ligament within porous structure were l = 6.67 mm and a = 0.66 mm, respectively. According to the theoretical design, the porous aluminum structure with 90% porosity was manufactured. Detail calculations of its structural parameters have been provided in [30]. The superiority of porous material fabricated by 3D printing is the controllability of shape and size. The commercially available paraffin RT42 (RUBITHERM, Germany) was selected as PCM. The employed PCM features the considerable latent heat, stable thermal performance and low phase transition temperature, which conduces to reducing heat loss in the experiment process. The thermal-physical properties of paraffin and metal materials are listed in Table 1.

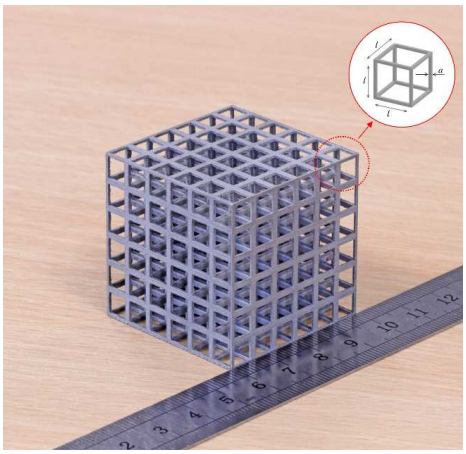

Fig. 1. Porous aluminum structure used for thermal performance enhancement

Table 1

Thermo-physical properties [34, 35]

Property	RT42 paraffin	Aluminum alloy	Copper alloy	Stainless steel	Titanium alloy
Specific heat, C (J/kg K)	2000	940	370	500	560
Density, ρ (kg/m^3)	880/760	2670	8910	8000	4430
Thermal conductivity, k (W/m K)	0.2	183	340	15	7.1
Viscosity, μ (kg/m s)	0.0235				

Thermal expansion coefficient, β (1/K)	0.0001
Latent heat, L (kJ/kg)	165
Solidus temperature, T_{m1} (K)	311
Liquidus temperature, T_{m2} (K)	315

2.2. Experimental setup and procedure

As depicted in Fig. 2, the experimental setup was built to examine the thermal performance of PCM with and without PMS in terms of solid-liquid interface evolvement, temperature variation and total melting time. The apparatus mainly consisted of test section, heating system, data measurement and collection system, and snapshot image system. The test section was composed of rectangular enclosure container, test sample and insulation material. The HD camera was employed to capture snapshots of melting interface through transparent plexiglass at a certain time interval. An electric copper heater with size of 40 mm×40 mm×1 mm was employed. The heater was mainly made of copper, which is conducive to providing uniform heat flux during the experiment. The constant power was supplied to heater by DC power for the heating system, where the power can be determined by recording the electric voltage and current. For current experiments, eleven pre-calibrated K-type micro-thermocouples with a wire diameter of 0.127 mm were utilized along the vertical mid-plane of container. Two typical locations (the center of composite PCM and heater) were selected to trace temperature variation of heated wall and metal structure, in which thermocouples were attached to copper heater and metal skeleton using thermal adhesive. In order to determine heat loss from side wall, eight thermocouples were attached to inner surface of insulation material using thermal tape. The last thermocouple was used to obtain ambient temperature. The temperature data at different locations were traced at every 1 s via the data logger, and then stored in PC for further investigation.

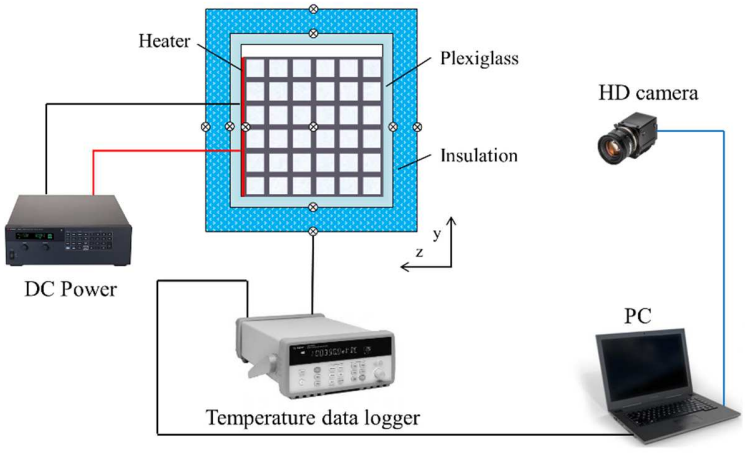

Fig. 2. Schematic illustration of experiment setup

A schematic diagram of test section is displayed in Fig. 3. The aluminum structure/paraffin composite PCM with size of 40 mm×40 mm×40 mm was used as test sample. Composite

PCM was prepared by impregnating porous aluminum structure with paraffin. To ensure that the pore cavity of PMS was filled with paraffin, the impregnation process was carried out in a vacuum, and the detailed method of preparation has been described in [36]. The cubic pure paraffin with the same size was also employed as test sample for a comparative test. The insulation material (polyurethane foam with 0.02 W/m K) was used to wrap plexiglass container for minimizing heat loss, where the internal dimensions of insulation cavity were based on the external size of plexiglass container. We found that the material of enclosure container had a significant effect on the melting evolvement of PCM by making some test. The relative lower thermal conductivity plexiglass (0.2 W/m K) is recommended rather than quartz glass. Thus, the rectangular enclosure container was made of plexiglass with a thickness of 3 mm. The about 5 mm gap between the top face of PCM and the inner surface of plexiglass was given for considering the volume expansion of paraffin during phase change process. Four small round holes were drilled through the top wall of plexiglass, which was used for releasing the pressure within enclosure container as well as conducive to fixation of wires of thermocouples and heater. The front face of insulation cavity was removed for about 20 s for tracing snapshot of melting interface at selected time interval.

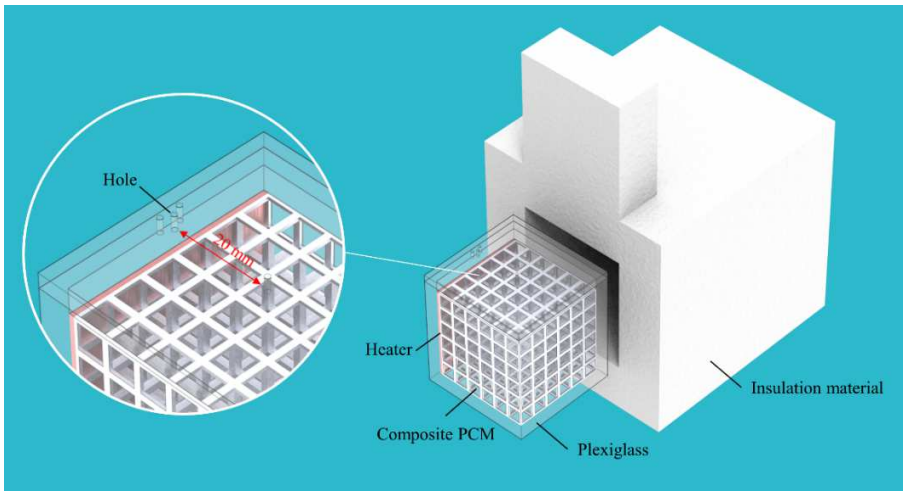

Fig. 3. Schematic illustration of the test section

2.3. Uncertainty analysis

The experimental uncertainty is determined in this section. The uncertainties of experiment are mainly caused by the errors of employed instruments, including the DC power, electric heater, and thermocouples. The uncertainties in DC power (U_{power}) and electric heater (U_{heater}) are 1% and 5%, respectively, as offered by manufacturers. The deviation of thermocouple (ΔT) connected with data collection system is ± 0.5 ℃. In addition, heat dissipation through insulation material should be considered for experimental uncertainty. Based on the one-dimensional Fourier law, the heat loss (Q_{loss}) can be evaluated according to the temperature data of thermocouples attached to insulation cavity. The power input (Q_{input}) supplied by DC power is

6.4 W. The overall uncertainty of experiment can be determined at 6.8% according to the following equation:

$$U=\sqrt{U_{\text{power}}^2+U_{\text{heater}}^2+\left(\frac{\Delta T}{T_{\text{ave}}}\right)^2+\left(\frac{Q_{\text{loss}}}{Q_{\text{input}}}\right)^2}\times 100\% \tag{1}$$

where T_{ave} is the time-averaged surface temperature.

3. Numerical simulation

3.1. Numerical method

The pore-scale numerical simulation is employed to investigate heat transfer mechanism in current study. Fig. 4 presents the schematic diagram of computational domain of PCM infiltrated in PMS, in which numerical models of PCM with and without PMS are reconstructed according to the test sample. In order to accurately simulate the physical problem of experiment, the numerical model considers the configuration of plexiglass container with 3 mm thickness and copper heater with 1 mm thickness. Thus, the computational domain with overall size of $46\ \text{mm}\times 46\ \text{mm}\times 47\ \text{mm}$ is established. Meanwhile, the following assumptions are adopted in present numerical simulation: (1) The flow of liquid paraffin in PMS is laminar flow and subjected to the Boussinesq approximation; (2) The thermo-physical properties of metal structure and paraffin are constant, and the volume variation of PCM is neglected; (3) The heat transfer coefficient is assumed to be constant for simulation of heat loss caused by convective heat transfer between insulation material and ambient.

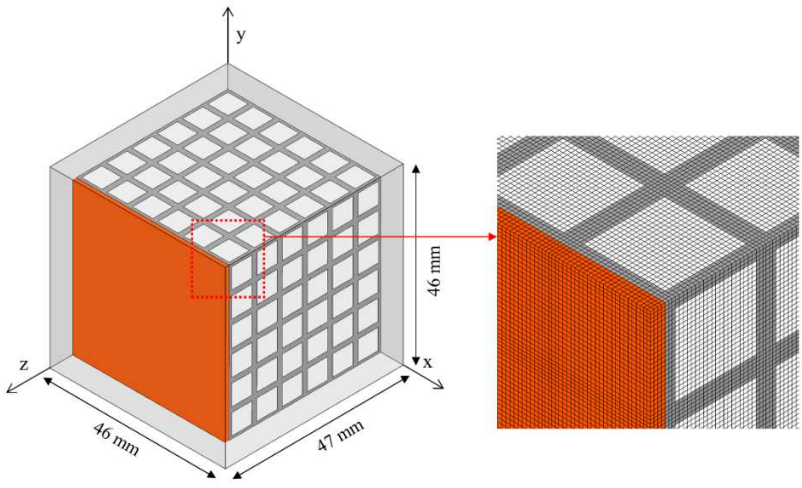

Fig. 4. Computational domain and representative mesh of composite PCM with plexiglass enclosure

According to the above assumptions, the governing equations of numerical model can be written as follows:

Continuity equation:

$$\nabla \cdot \vec{u}=0 \tag{2}$$

Heat transfer in composite PCM is complex, and mainly consists of conduction, phase change, and heat convection. The conduction heat transfer in the entire computational region can be defined by:

$$\rho C \frac{\partial T}{\partial t} = \nabla \cdot \left(k \nabla T \right) + \dot{q} \tag{3}$$

where $\dot{q}$ is heat generation rate of heat source (i.e., copper heater).

Momentum equation:

$$\rho_p \frac{\partial \vec{u}}{\partial t} + \rho_p \left(\vec{u} \cdot \nabla \right) \vec{u} = -\nabla P + \mu_p \nabla^2 \vec{u} + \rho_p g \beta \left(T_p - T_m \right) + S\vec{u} \tag{4}$$

where $\vec{u}$ is velocity vector of liquid phase PCM.

The momentum term $S\vec{u}$ in Eq. (4) is used to damp velocity in solid phase domain, where S is given by:

$$S = \frac{\left(1 - f_l\right)^2}{c + f_l^3} A_{\text{mush}}$$

(5)

where A_{mush} is a mush zone constant between 10^4 and 10^7 which is recommended in [37], $A_{\text{mush}} = 10^5$ is selected in the present study [25]. c is a small constant set to 0.001 to avoid zero in the denominator. f_l is liquid fraction between 0 and 1, which can be determined by:

$$f_l = \begin{cases} 0 & T_p < T_{m1} \\ \left(T_p - T_{m1}\right) / \left(T_{m2} - T_{m1}\right) & T_{m1} < T_p < T_{m2} \\ 1 & T_p > T_{m2} \end{cases} \tag{6}$$

Heat transfer in solid and liquid regions of PCM can be governed by:

$$\rho_p C_p \frac{\partial T_p}{\partial t} + \rho_p C_p \vec{u} \cdot \nabla T_p = \nabla \cdot \left(k_p \nabla T_p \right) - \rho_p L \frac{\partial f_l}{\partial t}$$

(7)

Heat transfer in metal structure is described as:

$$\rho_s c_s \frac{\partial T_s}{\partial t} = \nabla \cdot \left(k_s \nabla T_s \right) \tag{8}$$

Temperature and heat flux continuity is defined at the interface of PCM and metal structure, as the following equations:

$$T_p = T_s \tag{9}$$

$$k_p \frac{\partial T_p}{\partial n} = k_s \frac{\partial T_s}{\partial n} \tag{10}$$

3.2. Initial and boundary conditions

The initial temperature of PCM with and without PMS is measured by thermocouples inserted in sample. The initial temperature is equal to ambient temperature $T_0 = 20$ ℃. The initial conditions can be expressed as follows:

$$T_p = T_s = T_0, \ 0 \leqslant x \leqslant 46, 0 \leqslant y \leqslant 46, 0 \leqslant z \leqslant 47 \tag{11}$$

Although outer surfaces of enclosure container are wrapped by insulation material, the heat loss should be considered in numerical simulation. Thus, outer surfaces of model are set as convective boundary conditions. The boundary conditions for the governing equations are represented by the following equations:

$$-k \frac{\partial T}{\partial x} = h_w (T_w - T_0), \quad x = \{0, 46\}, \ 0 \leqslant y \leqslant 46, 0 \leqslant z \leqslant 47 \tag{12}$$

$$-k \frac{\partial T}{\partial y} = h_w (T_w - T_0), \ 0 \leqslant x \leqslant 46, \quad y = \{0, 46\}, \ 0 \leqslant z \leqslant 47 \tag{13}$$

$$-k \frac{\partial T}{\partial z} = h_w (T_w - T_0), \ 0 \leqslant x \leqslant 46, 0 \leqslant y \leqslant 46, \quad z = \{0, 47\} \tag{14}$$

Where T_w is wall temperature. Convective heat transfer occurs between insulation material and ambient air, in which the heat transfer coefficient can be estimated using empirical correlations [38]:

$$h_1 = \frac{0.62 k_{air}}{D} (GrPr)^{1/5} \tag{15}$$

$$h_2 = \frac{0.59 k_{air}}{D} (GrPr)^{1/4} \tag{16}$$

3.3. Numerical procedure

The CFD software Fluent 18.0 is used to perform pore-scale numerical calculation. The momentum and energy equations are discretized using second order upwind schemes. PISO algorithm is employed for coupling velocity and pressure field. The PRESTO method is adopted for calculation of pressure term. ICEM CFD 18.0 is used for dividing computational domain of model. The grids of computational domain are generated using a structured hexahedron element. The structured grids can reduce computation time and improve computation accuracy. Details of

the meshes of metal structure and paraffin are presented in Fig. 4, where the mesh of plexiglass domain is omitted for clarity. The grid independence test is performed for validating accuracy of numerical calculation. Two different numbers of grids (coarse grid with 3156k cells and fine grids with 6735k cells) are tested. The liquid fraction of composite PCM with different grids is compared, as shown in Fig. 5. It is observed that numerical results of two grids are almost the same and the deviation of results is less than 1%. In order to ensure accuracy of calculation and reduce computational time, the grid of 3156k cells is selected. In addition, power density of copper heater is set as 4e6 W/m^3 in numerical calculation according to power input of experiment.

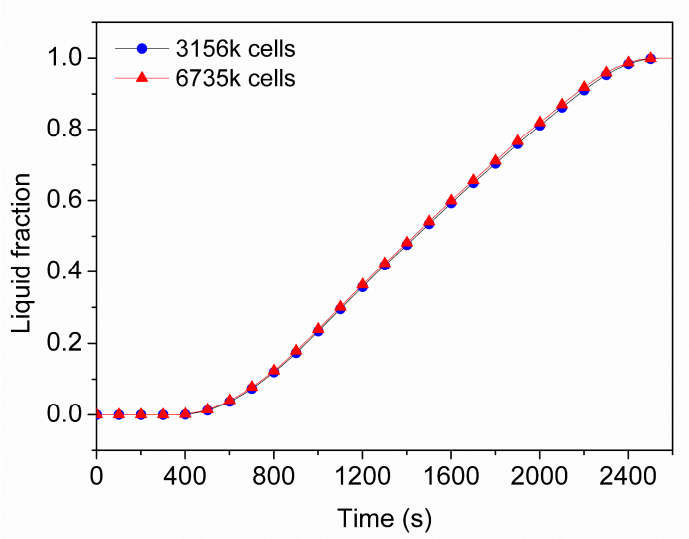

Fig. 5. Mesh independence test

4. Results and discussion

4.1. Solid-liquid interface and melting fraction

Fig. 6 presents the experimental and numerical results of the evolution of solid-liquid interface for PCM with and without PMS at the central plane (i.e., the plane of x = 23 mm) at 15 min, 25 min, and 35 min. Fig. 6(a) depicts experimental results of melting interface of pure paraffin. It is observed that melting interface is slightly crooked at 15 min, which indicates that natural convection and heat conduction have comprehensive impact on heat transfer during melting. As the melting progresses, the incline of melting interface of paraffin is more obvious, which indicates the natural convection develops and gradually dominates heat transfer in melting phase change. In the later stage of melting, the curvature of melting interface is very lager, and melting of pure paraffin at the right bottom domain is slow until paraffin becomes completely liquid phase after about 68 min. We can find that numerical results agree well with experimental results, as presented in Fig. 6(b).

The experimental results of melting interface of PCM with PMS are shown in Fig. 6(c). In the early stage of melting, melting interface of composite PCM is parallel to heated wall, which

is attributed to that heat conduction plays a significant role in melting heat transfer. As the melting continues, solid-liquid interface remains nearly straight at 25 min, in contrast to the scenario during the melting of pure paraffin. This phenomenon reveals that melting heat transfer within composite PCM is still dominated by heat conduction. The melting interface slightly slopes at the later stage of melting evolution, which represents the natural convection within composite PCM is strengthened and has an effect on melting evolvement of composite PCM until paraffin completely melts after about 42 min. Red in the figure below represents the zone of liquid phase, and blue represents that of solid phase. The transitional color between blue and red stands for the mushy zone, as displayed in Fig. 6(d). It is observed that the numerical results obtained using pore-scale numerical method are in good agreement with experimental results at the same time.

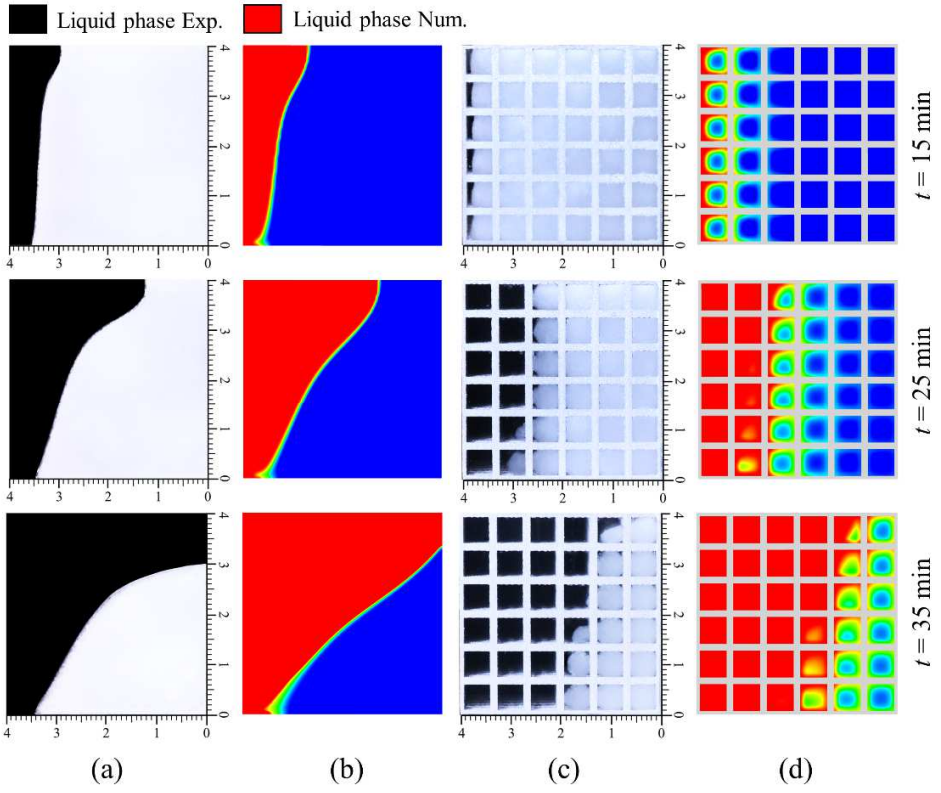

Fig. 6. Evolvement of solid-liquid interface (a) pure paraffin (Exp.), (b) pure paraffin (Num.), (c) composite PCM (Exp.) and (d) composite PCM (Num.)

To further examine the enhancement in the thermal performance of PCM, the numerically predicted results of liquid fraction of PCM with and without PMS are shown in Fig. 7. At the beginning of melting process, heat accumulates at the domain near heated wall owing to low thermal conductivity of pure paraffin. The temperature close to heated wall quickly reaches melting point and pure paraffin begins to melt. By contrast, the paraffin with PMS begins melting when heated for 500 s, which is attributed to the faster heat transfer within composite

PCM owing to high thermal conductivity PMS. Hence, the liquid fraction of paraffin with PMS is smaller than that of pure paraffin before about 1000 s. However, it is noted that the rate of melting of composite PCM is larger than that of pure paraffin in phase change process. Although pure paraffin initially melts sooner than paraffin with PMS, the total melting time of paraffin with PMS is shorter and decreased by 38% compared with paraffin without PCM. The deviation of total melting time obtained between the numerical simulation and experimental measurements is within 2%. For instance, for composite PCM, the numerical result for total melting time is 2555 s and experimental data is 42 min (i.e., 2520 s).

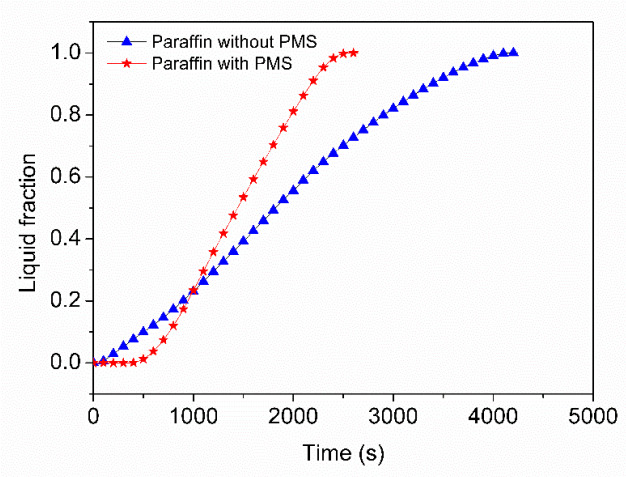

Fig. 7. Comparison of liquid fraction

4.2. Comparison of the temperature

Fig. 8 illustrates the comparison of numerical results and experimental data of temperature variation of composite PCM at two measurement points, TC#1 (y = 23 mm, z = 43 mm) and TC#2 (y = 23 mm, z = 23 mm). The melting process within composite PCM can be divided into three stages: the pre-melting stage, melting stage and post-melting stage. In the pre-melting stage, the temperature is below the melting point of paraffin and the increasing rate of temperature is high. In the melting stage, considerable heat is stored in paraffin by the latent heat, and the temperature rises at a lower rate. When the melting of paraffin is completed (i.e., post-melting stage), the increasing rate of temperature becomes large again. Moreover, it is found that the rate of temperature rise at two monitoring points is almost the same, which is due to the heat is stored by sensible heat at that time. The root mean squared error (RMSE) can be used for measuring the differences between predicted values and experimental data. The RMSE is calculated by $\mathrm{RMSE} = \sqrt{\frac{1}{n}\sum_{i=1}^{n}\left(\hat{y}_i - y_i\right)^2}$, where y_i are the experimental data, and $\hat{y}_i$ are the predicted value.

For current study, the overall RMSE in the temperature is 1.2 °C, which indicates numerical results exhibit good agreement with experimental data.

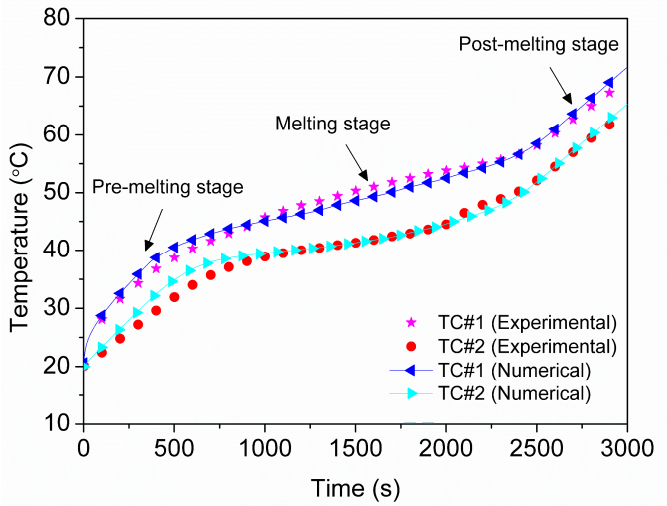

Fig. 8. Comparison of numerical and experimental data for temperature

To better present the thermal performance enhancement of PCM, a comparison of temperature fields of PCM with and without PMS is shown in Fig. 9. It is clearly found from Fig. 9(a) that temperature of liquid paraffin close to heated face remains high, while that of solid paraffin at right bottom part remains constant at the initial temperature of 293K in the whole melting process, which exhibits the temperature non-uniform within pure paraffin. Conversely, temperature field of composite PCM is uniform compared to pure paraffin at the same time, as depicted in Fig. 9(b). This is because heat can be quickly transferred from hot wall to the whole domain of composite PCM through high thermal conductivity metal structure. The numerically precited result indicates the maximum temperature difference of PCM embedded in PMS is decreased by about 81% compared with pure paraffin in phase change process.

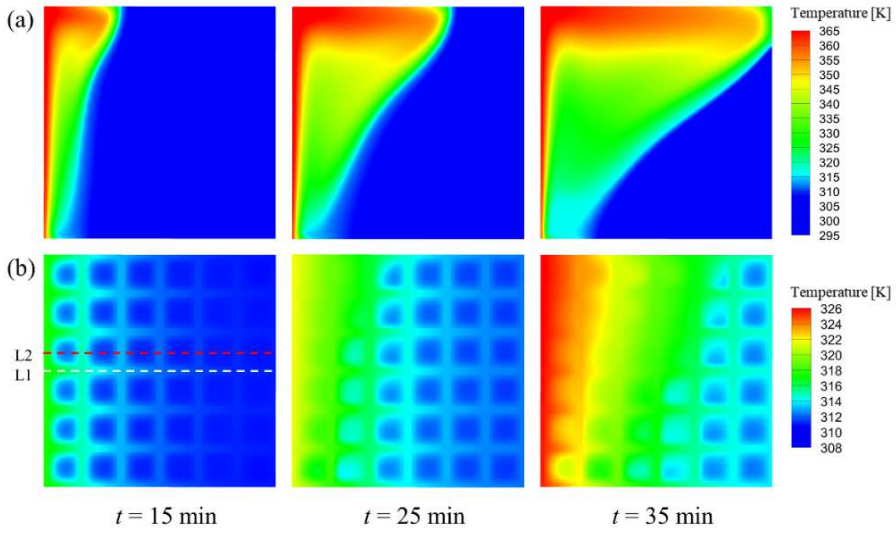

Fig. 9. Temperature field of (a) pure paraffin, (b) composite PCM

It can be observed that there is local thermal non-equilibrium between metal structure and paraffin, as presented in Fig. 9(b). To visibly illustrate heat transfer characteristic of composite PCM, Fig. 10 shows temperature variation along two horizontal lines (L1 of y = 23 mm, and L2 of y = 26.3 mm) drawn in Fig. 9(b). It is found that temperature of composite PCM along L1 drops gradually from hot wall to cold wall, which is owing to L1 is located in high thermal conductivity metal ligament, and heat is transferred by heat conduction. However, it can be noticed that temperature variation of composite PCM along L2 exhibits periodic fluctuation, which is caused by the difference in thermal conductivities between PCM and PMS. Furthermore, the local temperature difference ΔT between metal structure and paraffin is obvious, where this is larger close to heated wall than away from it.

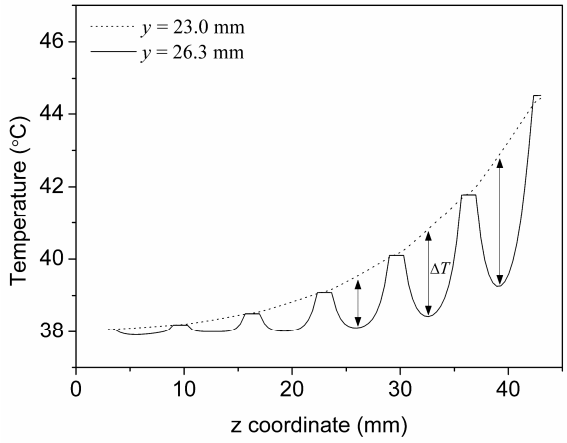

Fig. 10. Temperature variation along two horizontal lines

4.3. Comparison of the velocity

To facility better understanding of heat transfer mechanism, the velocity field of pure paraffin and composite PCM is displayed in Fig. 11. Fig. 11(a) depicts the velocity field of pure paraffin on the plane of x = 23 mm. Due to the effect of buoyancy force, liquid paraffin near heated wall flows upward, and ascends to the top part. Then liquid paraffin flows downward along melting interface, which yields a circulating current in the liquid region of paraffin. This reveals that natural convection plays a vital role in melting heat transfer for pure paraffin. It is found that the flow of liquid paraffin is most distinct at 15 min. the velocity of liquid paraffin adjacent to heated wall and melting interface is larger than that of other domain during the melting process. Moreover, it is seen that the maximum velocity within pure paraffin is larger than that within composite PCM, which is due to the larger flow resistance resulted from embedding PMS.

The velocity fields of paraffin with PMS on the planes of x = 26.3 mm and x = 23 mm are illustrated in Figs. 11(b) and 11(c), respectively. It is found that the velocity of liquid paraffin at x = 23 mm is very small during the whole melting process. This is due to the liquid paraffin on this plane is divided into small regions by metal structure, which leads to higher flow resistance. The

liquid paraffin forms a faint flow within the cell structure. The velocity of liquid paraffin (x = 26.3 mm) is more obvious compared to the liquid paraffin (x = 23 mm). It is found that velocity of molten paraffin is close to 0 m/s in the initial stage, which demonstrates heat transfer in PCM with PMS is dominated by heat conduction in this period. As the melting continues, flow of liquid paraffin driven by buoyancy gradually develops and its velocity is becoming larger, which indicates that natural convection starts to occur. It can be found that the flow of liquid paraffin can also form a circulating current in the post-melting stage, which represents that natural convection is strengthened, as analyzed in Section 4.1. Furthermore, we can find some small circulating current around the metal struts (denoted by the circle), which can strengthen heat exchange between the metal structure and paraffin. According to the above analysis, it is proved that there is some difference in heat transfer mechanism between pure paraffin and composite PCM.

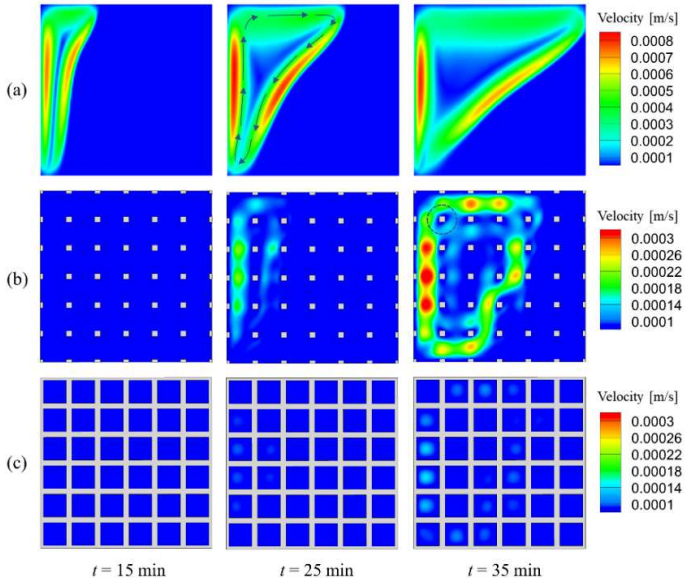

Fig. 11. Velocity fields of (a) pure paraffin, (b) composite PCM (x = 26.3 mm), and (c) composite PCM (x = 23 mm)

4.4. Analysis of energy storage

To estimate the thermal storage performance of PCM with and without PMS, we perform the analysis of energy storage rate (i.e., per unit time per mass of PCM stores energy). The energy (E) stored from the beginning of heating to the completion of melting can be calculated by the following equation [39]:

$$E_p(t)=\begin{cases} m_p C_p (T_p(t)-T_0) & T_p < T_m \\ m_p C_p (T_p(t)-T_m)+m_p L+m_p C_p (T_m-T_0) & T_p > T_m \end{cases} \tag{17}$$

where E_p is the energy stored in paraffin, t is the total melting time, and T_p is the average temperature of paraffin.

Based on the numerical simulation and above theoretical calculation, a comparison of energy storage is shown in Table 2. It is found that energy stored in PMC with PMS is smaller than that of PCM without PMS, which can be attributed to the fact that embedding PMS results in a reduction in the mass of paraffin. However, it is seen from results that the energy storage rate of paraffin without PMS is 74.7 J/kg s, and the energy storage rate of paraffin with PMS is 90.3 J/kg s. The energy storage rate thus improves 1.2 times by embedding porous metal structure.

Table 2
Comparison of energy storage

	Melting time, t (s)	Energy, E (J)	Energy storage rate (J/Kg s)
PCM with PMS	2555	11692	90.3
PCM without PMS	4153	17464	74.7

4.5. Effect of metal material

Fig. 12 shows the comparison of liquid fractions of PCM embedded in PMS with four materials. It can be found that the variation tendencies in liquid fraction for composite PCM with different materials are similar, i.e., the liquid fraction of composite is zero in the pre-melting stage, and gradually increases until melting completes. The melting rate of composite PCM is different, where the melting rate of PCM with porous copper structure is the highest among embedding the four materials. It is demonstrated that the material with a high thermal conductivity is better conducive to enhancing the heat transfer performance of PCM, e.g., total melting time of PCM embedding copper structure can be reduced by 42% compared to embedding titanium alloy structure.

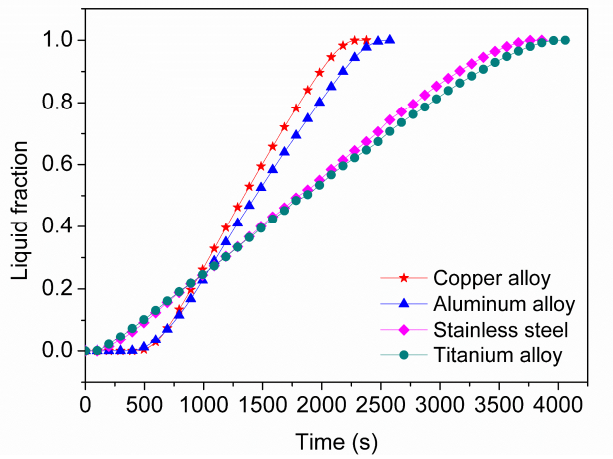

Fig. 12. Comparison of liquid fractions of PCM embedded in PMS with four materials

The liquid fraction of pure paraffin is selected as benchmark, and the enhancement ratio of PCM embedded in four metal materials can be defined by:

$$e_r = \left[\frac{f_l(\text{composite})}{f_l(\text{paraffin})} \text{-1} \right] \times 100\% \tag{18}$$

To facilitate quantitative comparison of thermal performance enhancement of PCM, the enhancement ratio e_r in the whole melting process is depicted in Fig. 13. At the beginning of melting, e_r is negative value for four porous metal materials, which means melting rate of PCM infiltrated in PMS is smaller than that of pure paraffin. This is because heat is more quickly transferred from heated wall to the whole domain of composite through metal ligament, and the temperature of paraffin near heated wall doesn't reach melting point. As time continues, e_r rises quickly and becomes positive value, which indicates that the rate of melting of PCM with PMS is larger compared to pure paraffin. It is noticed that the effect of embedding aluminum structure and copper structure on the thermal performance enhancement of PCM is significant, in which maximum e_r for PCM with copper structure can reach 63%. Furthermore, it is found that the e_r for composite PCM with stainless steel and titanium alloy is small, which reveals the role of embedding low conductivity metal structure in the thermal performance enhancement of PCM is negligible.

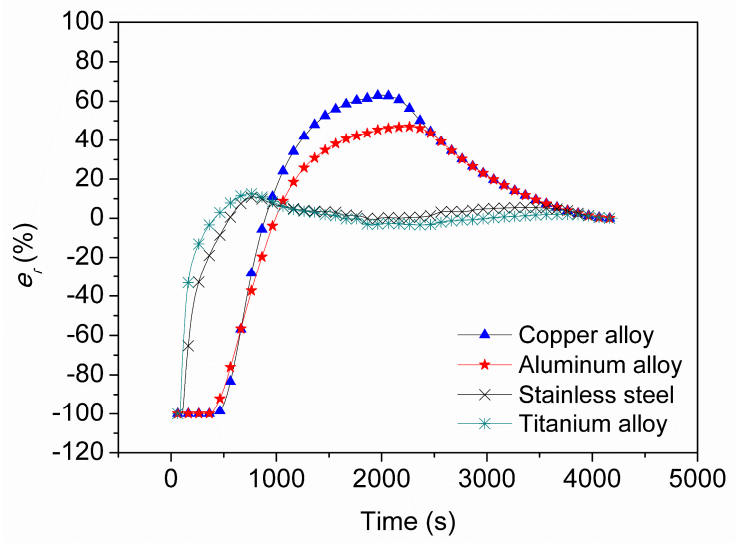

Fig. 13. Comparison of enhancement ratios e_r of PCM embedded in PMS with different materials

5. Conclusion

In this paper, the thermal performance enhancement of PCM was experimentally and numerically investigated. Composite PCM was fabricated by embedding a porous aluminum structure in paraffin. The visible experiment was conducted to study thermal performance enhancement of PCM, in which the PMS fabricated by 3D printing was used as heat transfer enhancer. Based on the pore-scale numerical method, the 3D model was developed to further investigate heat transfer characteristics of PCM with and without PMS.

(1) It is demonstrated from experimental and numerical results that embedding PMS can

improve the thermal behavior of PCM, e.g., the total melting time of paraffin with PMS is shortened by 38% compared to pure paraffin. Moreover, the temperature field of paraffin with PMS is more uniform, e.g., maximum temperature difference of PCM with PMS can be decreased by about 81% compared to pure paraffin. In addition, it is found that the energy storage rate of PCM with PMS is improved 1.2 times that of pure paraffin. The numerically predicted results are in good agreement with experimental data.

(2) The heat transfer mechanics of paraffin with PMS are different from that of pure paraffin by analyzing the solid-liquid interface and velocity field, e.g., heat conduction plays an important role in the melting process of composite PCM. whereas, the melting heat transfer of pure paraffin is dominated by natural convection during the melting process. In addition, A temperature difference is observed between metal structure and paraffin, and local thermal non-equilibrium near hot wall is more obvious than that away from hot wall.

(3) Porous metal structure with different materials has different effects on the thermal performance of composite PCM. It is found that the use of high thermal conductivity PMS can drastically strengthen the thermal behavior of PCM, e.g., the maximum enhancement ratio of PCM with porous copper structure can reach 63%. However, embedding low thermal conductivity PMS has a minor effect on the thermal performance enhancement of PCM.

Acknowledgement

The authors thank China Scholarship Council (CSC) for providing a scholarship to conduct this study.

References

[1] E. Oro, A. de Gracia, A. Castell, M.M. Farid, L.F. Cabeza, Review on phase change materials (PCMs) for cold thermal energy storage applications, Appl. Energy. 99 (2012) 513-533.

[2] Y.B. Tao, Y.-L. He, A review of phase change material and performance enhancement method for latent heat storage system, Renew Sust Energ Rev 93 (2018) 245-259.

[3] Z. Khan, Z. Khan, A. Ghafoor, A review of performance enhancement of PCM based latent heat storage system within the context of materials, thermal stability and compatibility, Energy Convers. Manage. 115 (2016) 132-158.

[4] N.I. Ibrahim, F.A. Al-Sulaiman, S. Rahman, B.S. Yilbas, A.Z. Sahin, Heat transfer enhancement of phase change materials for thermal energy storage applications: A critical review, Renew Sust Energ Rev 74 (2017) 26-50.

[5] T. Li, J.-H. Lee, R. Wang, Y.T. Kang, Enhancement of heat transfer for thermal energy storage application using stearic acid nanocomposite with multi-walled carbon nanotubes, Energy 55 (2013) 752-761.

[6] X. Song, Y. Cai, C. Huang, Y. Gu, J. Zhang, H. Qiao, Q. Wei, Cu Nanoparticles Improved Thermal Property of Form-Stable Phase Change Materials Made with Carbon Nanofibers and LA-MA-SA Eutectic Mixture, Journal of Nanoscience and Nanotechnology 18 (2018) 2723-2731.

[7] S. Ramakrishnan, X. Wang, J. Sanjayan, Thermal enhancement of paraffin/hydrophobic expanded perlite granular phase change composite using graphene nanoplatelets, Energy and Buildings 169 (2018) 206-215.

[8] S. Ramakrishnan, X. Wang, J. Sanjayan, Effects of various carbon additives on the thermal storage performance of form-stable PCM integrated cementitious composites, Appl. Therm. Eng. 148 (2019) 491-501.

[9] B. Kamkari, D. Groulx, Experimental investigation of melting behaviour of phase change material in finned rectangular enclosures under different inclination angles, Exp. Therm Fluid Sci. 97 (2018) 94-108.

[10] A. Arshad, H.M. Ali, S. Khushnood, M. Jabbal, Experimental investigation of PCM based round pin-fin heat sinks for thermal management of electronics: Effect of pin-fin diameter, Int. J. Heat Mass Transfer 117 (2018) 861-872.

[11] R. Baby, C. Balaji, Experimental investigations on phase change material based finned heat sinks for electronic equipment cooling, Int. J. Heat Mass Transfer 55 (2012) 1642-1649.

[12] A. Jamekhorshid, S.M. Sadrameli, M. Farid, A review of microencapsulation methods of phase change materials (PCMs) as a thermal energy storage (TES) medium, Renew Sust Energ Rev 31 (2014) 531-542.

[13] W. Li, R. Hou, H. Wan, P. Liu, G. He, F. Qin, A new strategy for enhanced latent heat energy storage with microencapsulated phase change material saturated in metal foam, Sol. Energy Mater. Sol. Cells 171 (2017) 197-204.

[14] F. Zhang, Y. Zhong, X. Yang, J. Lin, Z. Zhu, Encapsulation of metal-based phase change materials using ceramic shells prepared by spouted bed CVD method, Sol. Energy Mater. Sol. Cells 170 (2017) 137-142.

[15] C.Y. Zhao, W. Lu, Y. Tian, Heat transfer enhancement for thermal energy storage using metal foams embedded within phase change materials (PCMs), Sol. Energy. 84 (2010) 1402-1412.

[16] X. Hu, F. Zhu, X. Gong, Experimental and numerical study on the thermal behavior of phase change material infiltrated in low porosity metal foam, J. Energy Storage 26 (2019) 101005.

[17] W.Q. Li, Z.G. Qu, Y.L. He, W.Q. Tao, Experimental and numerical studies on melting phase change heat transfer in open-cell metallic foams filled with paraffin, Appl. Therm. Eng. 37 (2012) 1-9.

[18] Z. Li, Z. Wu, Numerical study on the thermal behavior of phase change materials (PCMs) embedded in porous metal matrix, Sol. Energy. 99 (2014) 172-184.

[19] J. Tian, T. Kim, T.J. Lu, H.P. Hodson, D.T. Queheillalt, D.J. Sypeck, H.N.G. Wadley, The effects of topology upon fluid-flow and heat-transfer within cellular copper structures, Int. J. Heat Mass Transfer 47 (2004) 3171-3186.

[20] M.F. Ashby, A. Evans, N.A. Fleck, L.J. Gibson, J.W. Hutchinson, and H.N.G. Wadley, Metal foams: a design guide, Oxford, Butterworth-Heinemann, 2000.
[21] Y. Yao, H. Wu, Z. Liu, Z. Gao, Pore-scale visualization and measurement of paraffin melting in high porosity open-cell copper foam, International Journal of Thermal Sciences 123 (2018) 73-85.
[22] J. Chen, D. Yang, J. Jiang, A. Ma, D. Song, Research progress of phase change materials (PCMs) embedded with metal foam (a review), in: A. Rabiei (ed.) 8th International Conference on Porous Metals and Metallic Foams, Vol. 4, 2014, pp. 389-394.
[23] A. Mustaffar, D. Reay, A. Harvey, The melting of salt hydrate phase change material in an irregular metal foam for the application of traction transient cooling, Thermal Science and Engineering Progress 5 (2018) 454-465.
[24] X. Yang, S. Feng, Q. Zhang, Y. Chai, L. Jin, T.J. Lu, The role of porous metal foam on the unidirectional solidification of saturating fluid for cold storage, Appl. Energy. 194 (2017) 508-521.
[25] S.S. Feng, M. Shi, Y.F. Li, T.J. Lu, Pore-scale and volume-averaged numerical simulations of melting phase change heat transfer in finned metal foam, Int. J. Heat Mass Transfer 90 (2015) 838-847.
[26] P. Zhang, Z.N. Meng, H. Zhu, Y.L. Wang, S.P. Peng, Melting heat transfer characteristics of a composite phase change material fabricated by paraffin and metal foam, Appl. Energy. 185 (2017) 1971-1983.
[27] R. Tauseef ur, H.M. Ali, A. Saieed, W. Pao, M. Ali, Copper foam/PCMs based heat sinks: An experimental study for electronic cooling systems, Int. J. Heat Mass Transfer 127 (2018) 381-393.
[28] T.X. Li, D.L. Wu, F. He, R.Z. Wang, Experimental investigation on copper foam/hydrated salt composite phase change material for thermal energy storage, Int. J. Heat Mass Transfer 115 (2017) 148-157.
[29] K.S. Gopalan, V. Eswaran, Numerical investigation of thermal performance of PCM based heat sink using structured porous media as thermal conductivity enhancers, International Journal of Thermal Sciences 104 (2016) 266-280.
[30] X. Hu, X. Gong, Pore-scale numerical simulation of the thermal performance for phase change material embedded in metal foam with cubic periodic cell structure, Appl. Therm. Eng. 151 (2019) 231-239.
[31] T.D. Ngo, A. Kashani, G. Imbalzano, K.T.Q. Nguyen, D. Hui, Additive manufacturing (3D printing): A review of materials, methods, applications and challenges, Composites Part B: Engineering 143 (2018) 172-196.
[32] X. Wang, S. Xu, S. Zhou, W. Xu, M. Leary, P. Choong, M. Qian, M. Brandt, Y.M. Xie, Topological design and additive manufacturing of porous metals for bone scaffolds and orthopaedic implants: A review, Biomaterials 83 (2016) 127-141.
[33] J.-M. Nunzi, A. Merabtine, N. Gardan, J. Gardan, H. Badreddine, C. Zhang, F. Zhu, X.-L.

Gong, R. Bennacer, M. El Ganaoui, Experimental and numerical thermal analysis of open-cell metal foams developed through a topological optimization and 3D printing process, The European Physical Journal Applied Physics 83 (2018) 10904.
[34] Rubitherm GmbH, Data sheet, Rubitherm Technologies GmbH, Berlin, Germany, 2018.
[35] C.Z. Ji, Z. Qin, S. Dubey, F.H. Choo, F. Duan, Simulation on PCM melting enhancement with double-fin length arrangements in a rectangular enclosure induced by natural convection, Int. J. Heat Mass Transfer 127 (2018) 255-265.
[36] X. Xiao, P. Zhang, M. Li, Preparation and thermal characterization of paraffin/metal foam composite phase change material, Appl. Energy. 112 (2013) 1357-1366.
[37] ANSYS fluent software package: user's manual, 18.0, 2017.
[38] S. Yang, W. Tao, Heat transfer, 4th ed., Beijing, Higher Education Press, 2006.
[39] F. Zhu, C. Zhang, X. Gong, Numerical analysis on the energy storage efficiency of phase change material embedded in finned metal foam with graded porosity, Appl. Therm. Eng. 123 (2017) 256-265.